ImmunoHorizons

RESEARCH ARTICLE

Innate Immunity

Role of NLRP3 Inflammasomes in Monocyte and Microglial Recruitments in Choroidal Neovascularization

Blake W. Dieckmann,*[,1] Marcell E. Paguaga,*[,1] Gary W. McCollum,* John S. Penn,* and MD Imam Uddin*[,†]

*Department of Ophthalmology and Visual Sciences, Vanderbilt University School of Medicine, Nashville, TN; and
†Department of Biomedical Engineering, Vanderbilt University School of Engineering, Nashville, TN

ABSTRACT

Although the pathogenesis of choroidal neovascularization (CNV) is largely unknown in age-related macular degeneration (AMD), inflammasomes may contribute to CNV development and progression. To understand the role NLRP3 inflammasomes in CNV, we used *Ccr2*^{RFP}*Cx3cr1*^{GFP} dual-reporter mice and immunostaining techniques to confirm localization of NLRP3 inflammasomes in the laser-induced CNV (LCNV) lesions. Confocal microscopy was used to image and quantify LCNV volumes. MCC950 was used as NLRP3 inhibitor. ELISA and quantitative RT-PCR were used to confirm the activation of NLRP3 by monitoring the expression of IL-1β protein and mRNA in choroidal tissues from LCNV mice. In addition, NLRP3 ($^{-/-}$) LCNV mice were used to investigate whether NLRP3 inflammasomes contribute to the development of LCNV lesions. We observed that red fluorescent protein (RFP)–positive monocyte-derived macrophages and GFP-positive microglia-derived macrophages, in addition to other cell types, were localized in LCNV lesions at day 7 post–laser injury. In addition, NLRP3 inflammasomes are associated with LCNV lesions. Inhibition of NLRP3 inflammasomes, using MCC950, caused an increased Ccr2^{RFP}-positive macrophages, Cx3cr1^{GFP}-positive microglia, and other cells, resulting in an increase in total lesion size. NLRP3 ($^{-/-}$) LCNV mice showed significantly increased lesion size compared with age-matched controls. Inhibition of NLRP3 resulted in decreased IL-1β mRNA and protein expression in the choroidal tissues, suggesting that increased lesion size may not be directly related to IL-1β. *ImmunoHorizons*, 2024, 8: 363–370.

INTRODUCTION

Age-related macular degeneration (AMD) is a vision-threatening condition affecting older adults, often resulting in blindness, in developed countries (1,2). AMD is classified into two major forms: dry AMD and neovascular or "wet" AMD. Even though only 10% of AMD cases are wet, they contribute to ∼90% of the vision loss in AMD. A key characteristic of wet AMD is choroidal neovascularization (CNV) in the macula causing severe vision loss (3). Although the pathogenesis of CNV is largely unknown, inflammasomes may contribute to its onset and progression. Currently, CNV is managed by intravitreal administration of anti–vascular endothelial growth factor (VEGF) therapy. However, ∼50% of wet AMD patients exhibit an incomplete

Received for publication April 1, 2024. Accepted for publication April 29, 2024.

Address correspondence and reprint requests to: MD Imam Uddin, AA1324 Medical Center North, Vanderbilt University Medical Center, Nashville, TN 37232-8808. E-mail address: md.i.uddin@vumc.org

ORCIDs: 0000-0003-4355-3089 (M.E.P.); 0000-0001-8070-5841 (J.S.P.); 0000-0001-5611-9666 (M.I.U.).

[1]B.W.D. and M.E.P. contributed equally to this work and share first authorship.

This work was supported by National Institutes of Health Grants R01EY029693-01 (to M.I.U.) and R01EY023397-07 (to M.I.U. and J.S.P.), American Diabetes Association Grant 11-22-IBSPM-12 (to M.I.U.), a grant from the Carl Marshall Reeves & Mildred Almen Reeves Foundation (to M.I.U.), and Vanderbilt Vision Research Center NEI Core Grant P30-EY008126. This work was also supported in part by a funding to the Vanderbilt Eye Institute from the International Retinal Research Foundation. The funding organizations had no role in the design or conduct of this research.

B.W.D. and M.E.P. performed experiments, collected and analyzed data, and wrote the manuscript. G.W.M. and J.S.P. helped revising the manuscript. M.I.U. conceived and supervised the project, designed and performed experiments, and revised the manuscript.

Abbreviations used in this article: AMD, age-related macular degeneration; CNV, choroidal neovascularization; ERG, electroretinography; LCNV, laser-induced choroidal neovascularization; RFP, red fluorescent protein; VEGF, vascular endothelial growth factor.

The online version of this article contains supplemental material.

response to anti-VEGF drugs. NOD-, LRR-, and PYD-containing protein 3 (NLRP3) inflammasome, a macromolecular complex that forms and induces inflammation in response to pathogens and cellular damage, is associated with CNV lesions (4,5). However, the role of NLRP3 is largely unknown. We hypothesized that NLRP3 inflammasomes contribute to CNV by regulating monocyte and microglial migration into the subretinal space.

The NLRP3 inflammasomes consist of three components: 1) NLRP3, 2) apoptosis-associated speck containing a caspase recruitment domain, and 3) caspase-1. When NLRP3 inflammasome formation is triggered, it enzymatically activates proangiogenic cytokines such as IL-1β (6), which can promote other proangiogenic molecules such as VEGF. Fig. 1 highlights the key features of AMD and how macrophages may contribute to the progression of CNV by a mechanism regulated by NLRP3 inflammasomes. Activated NLRP3 inflammasomes are associated with macrophages that infiltrate into the CNV lesions in VEGF-A^{hyper} mice, a genetic mouse model of AMD (7). Genetic inactivation of NLRP3 in these VEGF-A^{hyper} mice reduced the number of CNV lesions (8). However, the role of NLRP3 inflammasomes in monocyte and microglial recruitment is not characterized. One major challenge to study the role of monocytes/microglia in AMD relates to the difficulties associated with distinguishing between peripheral monocyte–derived macrophages and resident microglia (9). In addition, both of these two cell types present common cell markers including F4/80 (7). In the current study, we have used *Ccr2*^{RFP}*Cx3cr1*^{GFP} dual-reporter mice in which resident microglia are tagged with GFP and circulating monocytes are tagged with red fluorescent protein (RFP). Therefore, we can distinguish between these two cell types while investigating the role of NLRP3 (10). To study the pathogenesis of AMD, several animal models have been reported in the literature (11). A reliable and reproducible model is laser-induced choroidal neovascularization (LCNV) (12). Despite missing key components of wet AMD, this model has been used in the development of therapies and the elucidation of molecular pathways in neovascularization (13). In this study, *Ccr2*^{RFP}*Cx3cr1*^{GFP} dual-reporter mice were tested using the LCNV protocol, allowing us to differentiate between resident microglia and monocyte-derived macrophages that are recruited to the CNV lesions (14). In addition, MCC950 is tested as NLRP3 inhibitor in the LCNV model using *Ccr2*^{RFP} *Cx3cr1*^{GFP} dual-reporter mice. MCC950 is an efficient NLRP3 inhibitor, which binds to NLRP3's NACHT domain and blocks the formation of the inflammasome complex. This inhibitor has been shown to alleviate symptoms in murine models of inflammatory diseases (15,16). Notably, MCC950 mitigated retinal neovascularization in murine diabetic retinopathy (17) and murine oxygen-induced retinopathy (18). In the current study, we examined the role of NLRP3 in monocyte recruitment and its effects on CNV developments.

MATERIALS AND METHODS

Reagents and drug formulations

All reagents were purchased and used as received unless otherwise indicated. MCC950 sodium salt was acquired from Selleckchem.com (Houston, TX; catalog no. S7809) and formulated to 4.4 mg/ml in a vehicle consisting of 10% DMSO (Sigma, Burlington, MA; catalog no. D8418) and 90% Dulbecco's PBS (Life Technologies, Waltham, MA; catalog no. 14190-144). Ketamine (NDC 0409-2051-15) was obtained from Hospira (Lake Forest, IL). Xylazine (NDC 593990110-20), proparacaine hydrochloride (NDC 17478-263-12), and fluorescein (NDC 17478-253-10) were acquired from Akorn (Lake Forest, IL). Tropicamide (NDC 61314-354-01) was purchased from Sandoz (Basel, Switzerland), and phenylephrine (NDC 42707-102-15) was obtained from Paragon BioTeck (Portland, OR). GenTeal Severe gel (0065-8064-01) was purchased from Alcon laboratories, Inc. (Fort Worth, TX).

Animals

C57BL/6J and B6.129(Cg)-Cx3cr1^{tm1Litt} Ccr2$^{tm2.1Ifc}$/Jern (Ccr2^{RFP} Cx3cr1^{GFP})J, and B6.129S6-Nlrp3^{tm1Bhk}/J mice were purchased from Jackson Laboratories (Bar Harbor, MA). At the time of LCNV induction, C57BL/6 mice and C57BL/6-J GFP/RFP mice were 8–10 wk old. The mice were group-housed according to their randomly assigned experimental treatment groups in ventilated cages maintained under a 12-h:12-h light:dark cycle at 22 ± 2°C within an institutional animal care facility. They were provided clean water (Nashville Metro Water Services, Nashville, TN) and a standard diet consisting of 4.5% fat (PicoLab Rodent Diet 5L0D; LabDiet, St. Louis, MO) ad libitum. They were humanely sacrificed by CO_2-induced asphyxiation followed by cervical dislocation.

Anesthesia, pupillary dilation, and corneal numbing

Anesthesia, pupillary dilation, and corneal numbing were performed prior to the following procedures: LCNV and electroretinography (ERG). Average 22-g-weight mice (n = 12 per group) were injected i.p. with a 70-μl solution consisting of a 1:1:2 mixture of ketamine (85.7 mg/kg):xylazine (17.9 mg/kg):saline. After induction of anesthesia, the pupils of the mice were dilated with a drop of 0.5% tropicamide and 2.5% phenylephrine. Their corneas were numbed with a drop of 0.5% proparacaine. Prior to the start of LCNV, the eyes were covered with GenTeal gel to maintain hydration during laser injury and imaging. For ERG measurements, the eyes were hydrated using artificial tears.

Laser-induced choroidal neovascularization

Bruch's membrane was ruptured with a laser using the Phoenix-Micron image guided laser system and the Phoenix-Micron IV retinal imaging system (Phoenix-Micron, Inc., Bend, OR). The mice were anesthetized, and the pupils were dilated as described above. Laser-induced Bruch's membrane rupture was created in four quadrants in each eye about two optic disc lengths away from the optic nerve head. Hemorrhage or irregular lesions were excluded. The laser settings for power, laser time, and diameter are 350 mW, 80 ms, and 50 μm, respectively. On day 4 after laser, the mice were sacrificed, and the

eyes were harvested, fixed overnight at 4°C, and dissected for immunostaining.

NLRP3 inhibition using MCC950

After induction of LCNV on day 0, the mice received i.p. injections of MCC950 (40 mg/kg) or vehicle for 6 days, starting 1 d after laser injury. The mice were sacrificed on day 7 for ex vivo analysis.

Electroretinography

On day 7 after MCC950 injection, the mice were dark-adapted overnight and assessed for retinal cell health using ERG. ERG measurements were performed according to our previously published methods (5). Briefly, after anesthesia, the mouse eyes were dilated as described above. The mice were place on a warm platform within the Ganzfeld dome of a Diagnosys LLC Espion electrophysiology system (Lowell, MA). The mice were then exposed to flashes of light ranging from −4 to 2 log cd·s/m^2, and the amplitudes of a-wave and b-wave were measured from baseline to peak. The amplitudes of the a-wave and b-wave were plotted as functions of luminance.

Molecular biology assays

RNA extraction was performed using the RNAeasy mini kit according to the manufacturer's protocol (Qiagen, Hilden, Germany, catalog no. 74106). cDNA synthesis was performed using a high-capacity cDNA reverse transcription Kit (Thermo Fisher Scientific, Waltham, MA, catalog no. 4368814) according to the manufacturer's protocol, using a MiniAMP Thermal Cycler (Thermo Fisher Scientific, Waltham, MA, catalog no. A37834). The cycling parameters are as follows: 50-μl sample, 105°C cover, 25°C for 10 min, 37°C for 2 h, 85°C for 5 min, and 4°C until sample collection. Quantitative RT-PCR was performed using QuantStudio 3 (Thermo Fisher Scientific, Waltham, MA, catalog no. A28567) using the following primers: β-actin control (Life Technologies, Carlsbad, CA, catalog no. 4351315), IL-1β (Thermo Fisher Scientific, Waltham, MA, catalog no. Mm00434228), and Vegfa (Thermo Fisher Scientific, Waltham, MA, catalog no. Mm01281447). The cycling parameters are as follows: Initial temperature to 95°C in 4.1°C/s, 20 s at 95°C, 1 s at 95°C, decrease of 3.17°C/s until 60°C, 20 s at 60°C, increase 4.14°C/s until 95°C, repeats 1 s, and 20-s intervals at 95°C and 60°C, respectively. A mouse IL-1β ELISA kit (Invitrogen, Waltham, MA, catalog no. MBS6002) was used to quantify IL-1β in the tissue samples. Manufacturer's protocol was followed. The eyes were enucleated, fixed in 10% neutral buffered formalin for 10 min, dissected (lens, cornea, iris removed, retina, choroid, and sclera remained), and homogenized in Pierce radioimmunoprecipitation assay buffer (Thermo Scientific, Waltham, MA, catalog no. 8900) using disposable pestles (Bel-Art, Wayne, NJ, catalog no. F199230001). Halt-protease inhibitor single-use cocktail 100× (Thermo Scientific, Waltham, MA, catalog no. 78430) was used as protease inhibitor.

Ex vivo imaging and three-dimensional reconstruction of LCNV lesion

On day 7 after laser injury, a total of 24 eyes per group, were harvested and fixed in 10% formalin at 4°C overnight, and then retinal pigment epithelium–choroid–sclera complex tissues were dissected. The tissues were blocked for 2–3 h in blocking solution (10% donkey serum, 1% BSA, 0.002% fish collagen in wash buffer solution). Tissues from NLRP3 ($^{-/-}$) mice were stained with Dylight 647–conjugated isolectin B4 (catalog no. DL-1208-0.5, Vector Laboratories) at dilution 1:100. Tissues from one set $Ccr2^{RFP}Cx3cr1^{GFP}$ mice were stained with ICAM-2 primary Ab (BioLegend, catalog no. 105602) overnight at 4°C with 1:100 dilution and followed by a 90-min incubation with Alexa Fluor 647 anti-rat IgG (catalog no. A48272, Life Technologies) in a 1:100 dilution. Another set of $Ccr2^{RFP}Cx3cr1^{GFP}$ mice were stained with anti-NLRP3 (Invitrogen, MA5-32255) overnight at 4°C at 1:70, followed by a 90-min incubation with Alexa Fluor 647 Anti-rabbit IgG (catalog no. A31573, Life Technologies) in a 1:100 dilution. All tissues were washed after both primary and secondary Ab incubations. The tissues were washed three times for 5 min with wash buffer. Next, the tissues were flat-mounted on slides using Prolong Diamond antifade mounting medium with DAPI (catalog no. P36962, Invitrogen) and imaged using confocal microscopy. All confocal images were taken on a Zeiss LSM 710 AxioObserver microscope (Carl Zeiss AG, Oberkochen, Germany) using EC Plan-Neofluar 20×/o.50 M27 objective. For the $Ccr2^{RFP}$ $Cx3cr1^{GFP}$ tissues, images were taken using same parameters for all tissues. For the GFP channel, the parameters are as follows: 488-nm laser at 2% power; pinhole, 2.73 AU; and detector gain, 700. For the RFP channel, the parameters are as follows: 561-nm laser at 10% power; and detector gain, 750. For the 649 channel, the parameters are as follows: 633-nm laser at 2% power; and detector gain, 700.

Three-dimensional reconstruction of LCNV lesions was performed using IMARIS 10.0 (Oxford Instruments, Abingdon, UK). In brief, the images were converted from CZI files to Imaris files using the Imaris image converter. The metadata were checked to make sure the images were converted correctly. For each channel (GFP, RFP, ICAM2-647), the surface creation tool was used for three-dimensional reconstruction. Surface creation (three-dimensional rendering) was performed automatically for all images and then each of the surfaces were examined to remove any background noise. The total number of voxels (pixels) of each three-dimensionally rendered surface was given by the software. This was converted to μm^3 by multiplying the total number of voxels by voxel volume (1.0 μm × 1.24 μm × 1.24 μm). A total of 46–58 lesions from 24 eyes per group were used for the final data analysis. LCNV lesions with hemorrhage or irregular shapes were excluded from this analysis.

Statistical analysis

GraphPad Prism 9 was used to make all graphs and perform statistical analysis. Multiple comparison *t* tests were performed

https://doi.org/10.4049/immunohorizons.2400025

using the two-stage Benamini, Krieger, and Yekutieli method with $Q = 1\%$. The data are expressed as the means ± SEM.

Ethical approval

All animal procedures were approved by the Vanderbilt University Institutional Animal Care and Use Committee and were compliant with the Association for Research in Vision and Ophthalmology Statement for the Use of Animals in Ophthalmic and Vision Research, the National Research Council's Guide for the Care and Use of Laboratory Animals, and the ARRIVE guidelines.

Availability of data and materials

The data that support the findings of this study are available within the article and its supplementary information or upon reasonable request to the corresponding author.

RESULTS

NLRP3 is expressed in LCNV lesions

As shown in Fig. 1, key features of wet AMD include migration of monocyte-derived macrophages and microglial cells into the subretinal space. We observed that in *Ccr2*^{RFP}*Cx3cr1*^{GFP} dual-reporter mice and in WT C57BL/6J mice, the LCNV lesions were primarily composed of isolectin B4–positive cells (mostly endothelial cells), GFP^{+} microglia, and RFP^{+} monocyte–derived macrophages (Fig. 2). In addition, NLRP3 expression is associated with LCNV lesions (Fig. 2F–I).

NLRP3 inhibition increases choroidal neovascularization in LCNV animals

NLRP3 inhibition caused an increased in volumes of CNV lesions in LCNV animals at day 7 after laser injury (Fig. 3). *Ccr2*^{RFP} *Cx3cr1*^{GFP} dual-reporter mice were either given MCC950 (NLRP3 inhibitor) or vehicle control for 6 days, from days 1 to 6 after laser-induced damage to the Bruch's membrane. On day 7, the choroidal tissues were harvested, stained for IB4, mounted on slides, and imaged using confocal microscopy. We observed that LCNV lesions are primarily composed of isolectin B4–positive cells (mostly endothelial cells), GFP^{+} microglial cells, and RFP^{+} monocyte–derived macrophages in *Ccr2*^{RFP} *Cx3cr1*^{GFP} dual-reporter mice. There was a significant increase in volume of all these cells after NLRP3 inhibition, contributing to an overall increase in CNV lesion size (Fig. 3). To further confirm the role of NLRP3 inflammasomes in LCNV lesion size increase, NLRP3 ($^{-/-}$) mice were used. We observed that size of the LCNV lesions were significantly larger in NLRP3 ($^{-/-}$) mice compared with WT mice, suggesting that NLRP3 inflammasomes may have contributions to CNV lesions (Fig. 4). These observations are in agreement with the current literature, although the role of NLRP3 inflammasomes in monocyte and microglial recruitment to CNV lesions has not previously been investigated (19). Interestingly, MCC950-treated mice showed decreased levels of IL1β (Fig. 5A, 5B), a known proangiogenic molecule (20). NLRP3 activation leads to IL-1β production and may lead to downstream changes in VEGF expression (19). These observations suggest that the increased lesion size may not be directly related to IL-1β.

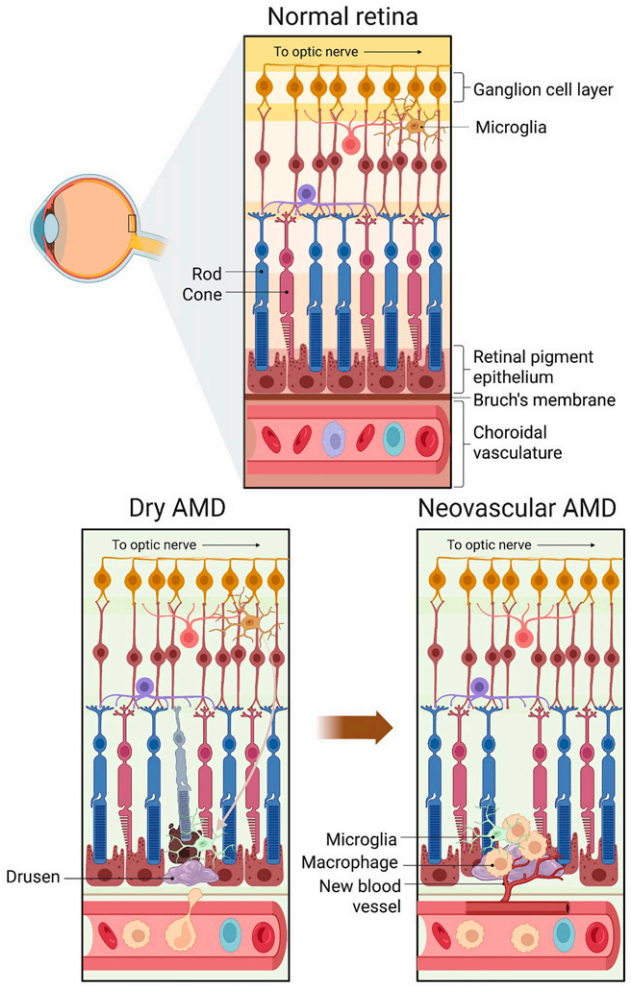

FIGURE 1.
Changes in retinal structures in early-stage or dry AMD and late-stage or neovascular AMD. In normal retina, microglia migrate into and out of the subretinal space. Dry AMD is associated with the accumulation of drusen in subretinal space, accumulation of microglia and macrophages, and a thickened Bruch's membrane. In neovascular AMD, Bruch's membrane breakdown leads to choroidal neovascularization (CNV), macrophage accumulation, and photoreceptor degeneration. Increased expression of NLRP3 inflammasomes is associated with AMD progression and could be an important target for molecular imaging of inflammation to predict the risk of CNV development and progression.

NLRP3 inhibitors has no effect on retinal cell functions

After NLRP3 inhibition using MCC950, we observed no significant changes in the a-wave and b-wave amplitudes in response to flashes of light intensities as a functional test to detect retinal cell health using ERG measurement at day 7 after laser injury (Fig. 5C). These data suggest that MCC950 has minimal effects on activation of other cells in the retina.

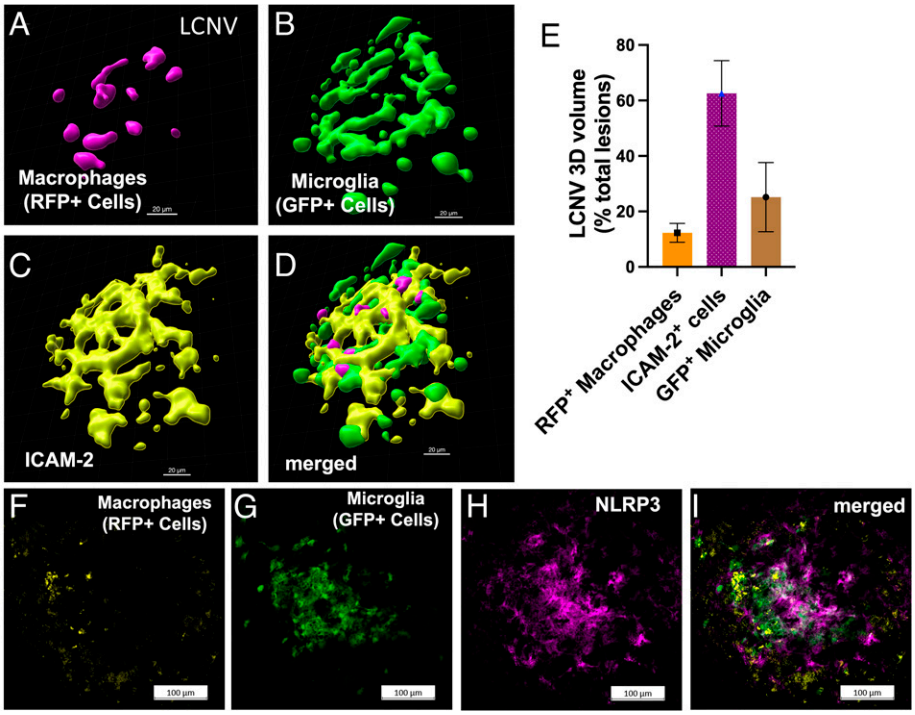

FIGURE 2.
Migration of macrophages and microglia and expression of NLRP3 inflammasomes in LCNV lesions. We used *Ccr2*^{RFP}*Cx3cr1*^{GFP} dual-reporter mice to characterize migration of Ccr2^{RFP}-positive macrophages and Cx3cr1^{GFP} positive microglia in LCNV at day 4 after laser injury. (**A**–**E**) Each LCNV lesion contains macrophages, ∼15% of the total LCNV volume; activated microglia, ∼20%; and ICAM-2 positive cells, ∼65% of the total LCNV lesion volume. (**F**–**I**) The immunofluorescence imaging shows that NLRP3 inflammasomes are associated with LCNV lesions at day 4 after laser injury. These are representative images of 10 LCNV eyes.

DISCUSSION

Wet AMD is a condition that is characterized by the key feature of CNV and currently is treated with agents that target VEGF. Even though they have proven beneficial effects in some cases, there is a large cohort of AMD patients that are refractory, resulting in disease progression and eventual vision loss (2). Therefore, understanding important drivers of choroidal neovascularization other than VEGF is necessary if outcomes are to ever be improved. In this study, we examine how NLRP3 inflammasomes, microglia, and monocyte-derived macrophages contribute to CNV development (7).

First, we wanted to confirm the importance of NLRP3 and its effect on CNV development. In *Ccr2*^{RFP}*Cx3cr1*^{GFP} mice, NLRP3 is expressed within the LCNV lesion as shown in Fig. 2. Next, NLRP3 ($^{-/-}$) mice were tested in the LCNV model to investigate the effects of NLRP3 activation on lesion volume. Indeed, NLRP3 knockout mice had an increase in lesion volume (Fig. 4). These data confirm a study by Doyle et al. (19) in which they also see an increase in lesion size in this same strain of mice. Though the protective role of NLRP3 against CNV development is still unclear, our data, in addition to the results of Doyle et al. (19), suggest that NLRP3 is protective. But in a mouse model in which VEGF-A^{hyper} mice are crossed with NLRP3-deficient mice, researchers found that there were more lesions (8). At first glance, these results seem conflicting, but these data actually suggest that NLRP3 might have different roles to play at different times in CNV development. It is possible that NLRP3 can promote the formation of CNV at an early stage, whereas at a different time, in a later stage of wet AMD for example, it can serve as protective role by decreasing CNV lesion size. The idea that the role of NLRP3 in CNV lesion formation versus progression could be different is further supported by the fact that there was no reported difference in lesion numbers in the VEGF^{hyper}/NLRP3 $^{(-/-)}$ mice compared with VEGF^{hyper} mice (7). This should be investigated further because it could affect the viability of NLRP3 as a drug target if its role shifts from detrimental to protective depending on the AMD progression.

To investigate the specific role(s) of NLRP3 on monocyte/microglial functions in CNV development, the *Ccr2*^{RFP}*Cx3cr1*^{GFP} dual-reporter mice were used. This mouse model allows resident microglia to be clearly distinguished from macrophages derived from circulating monocytes (10). Our data clearly showed that both microglia and monocyte-derived macrophages are recruited to lesions and are present at the peak CNV development at day 7 after laser injury (Fig. 3). Initially, these lesions were also stained with ICAM-2, a marker of endothelial cells (21), to help visualize the lesion's volume. In addition, IB4 was used to stain endothelial cells and other cells including microglia and macrophages, to visualize the LCNV volume (22,23).

The LCNV model in *Ccr2*^{RFP}*Cx3cr1*^{GFP} dual-reporter mice does have several limitations. Although *Ccr2*^{RFP}*Cx3cr1*^{GFP} dual-reporter mice have been used to study retinal degeneration (10), it is a double knockout/knock-in mouse model, so both *CCR2* and *Cx3cr1* have been deleted. Therefore, recruitment of monocytes through CCL2 signaling is impaired (Supplemental Fig. 1) (14). Cx3cr1 modulates microglia activation in various ways depending on the neurologic conditions (24). Therefore, microglia in this model could behave differently. Supplemental Fig. 2 shows changes in microglial morphology of the course of LCNV model. Despite these limitations, this model can still

https://doi.org/10.4049/immunohorizons.2400025

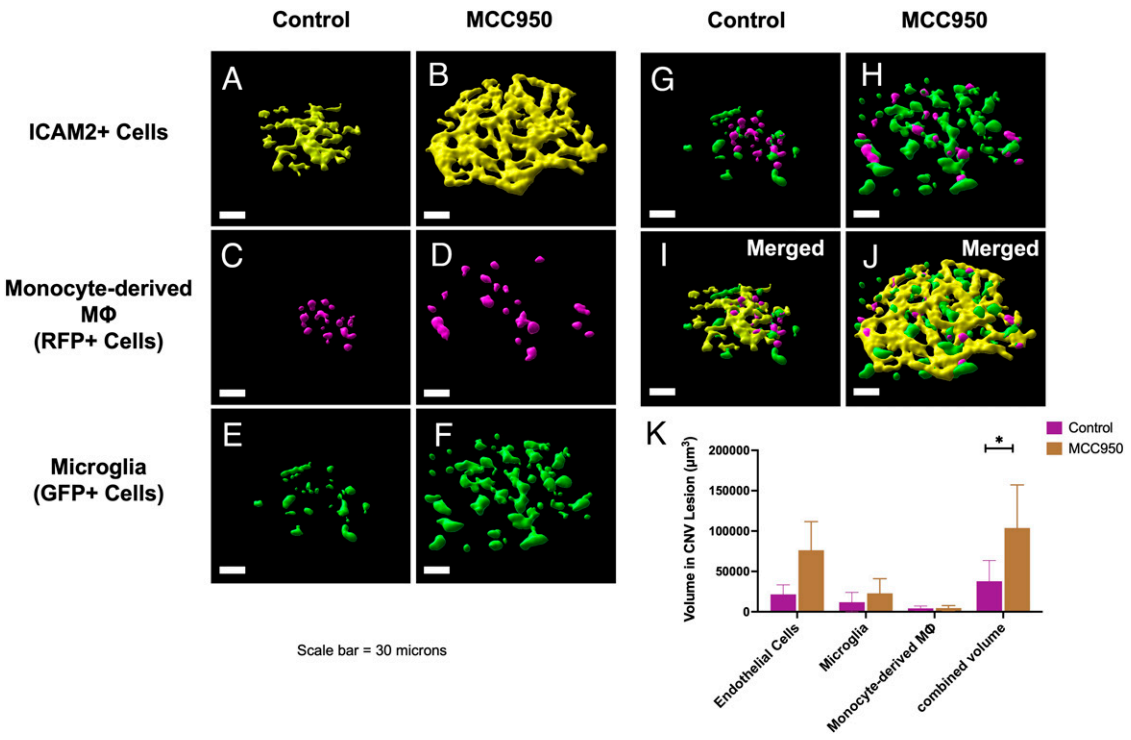

FIGURE 3.

Role of NLRP3 inflammasomes in monocyte and microglial migration. (**A**–**J**) Representative Imaris reconstructed confocal images of the CNV lesions from the control group and the MCC950-treated group. (**K**) Inhibition of NLRP3 inflammasomes using MCC950 leads to increases in total volume of ICAM-2+ cells, $Ccr2^{RFP}$-positive macrophages, and $Cx3cr1^{GFP}$-positive microglia, resulting in an increased lesion size. The volumes of the specific cells in LCNV lesions were analyzed from Imaris generated three-dimensional reconstruction of the corresponding confocal images. These are representative images of over 10 LCNV eyes ($n > 40$ lesions per group).

help show how monocytes are regulated by NLRP3 during choroidal neovascularization.

MCC950-treated mice have an increase in lesion volume compared with control mice (Fig. 3), similar to NLRP3 ($^{-/-}$) mice (Fig. 4). This increased lesion volume in Fig. 3 was due to significant increases in microglia, monocyte-derived macrophages, and $ICAM2^{+}$ cells. This suggests that NLRP3 plays a protective role against growth of CNV lesions, potentially by decreasing recruitment of monocyte-derived macrophages and microglia. Previous studies support this hypothesis by showing that lesion size decreases when macrophages are depleted (25,26). Other studies have shown that changes in microglia can contribute to CNV lesion size as well (27). In addition, recent evidence suggests that activation of NLRP3 may lead to pyroptosis in the retinal pigment epithelium–choroid tissues (28), and thus inhibition of NLRP3 activation may lead to inhibition of programmed cell death and ultimately contributing to increased CNV lesion size.

Finally, we looked at proangiogenic signaling molecules that are associated with NLRP3 and CNV lesions. An important

FIGURE 4.

Role of NLRP3 inflammasomes in monocyte migration in NLRP3 ($^{-/-}$) LCNV mice. (**A** and **B**) Representative confocal images of LCNV lesions in WT and NLRP3 ($^{-/-}$) respectively. (**C** and **D**) Corresponding Imaris generated three-dimensional reconstruction of the lesions ($n = 19$ and $n = 13$ for wild-type [WT] and NLRP3 [$^{-/-}$] mice, respectively). (**E**) The total volumes of LCNV lesions were larger than the wild-type age-matched controls.

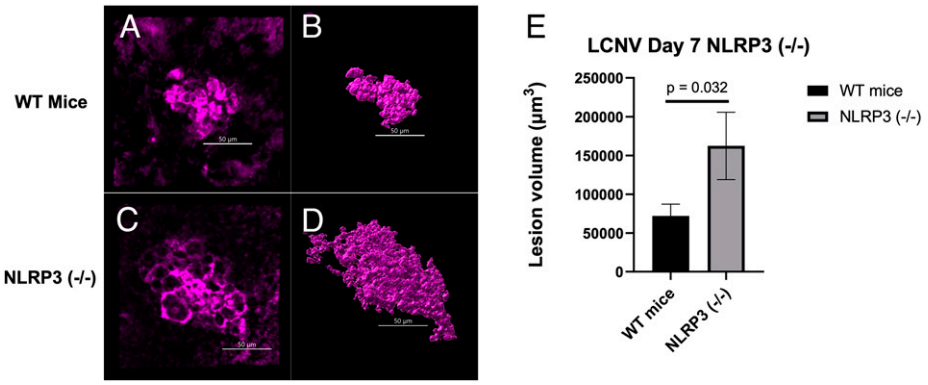

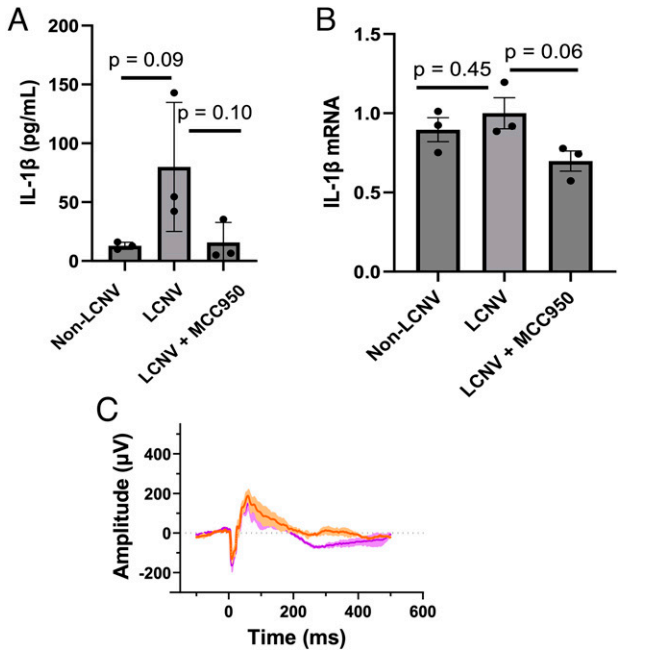

FIGURE 5.

Expression of IL-1β in choroidal tissues isolated from LCNV animals at day 7 after laser injury. (**A** and **B**) Both IL-1β protein and mRNA expressions were increased in LCNV tissues compared with nonlasered controls. Both IL-1β protein and mRNA expressions were decreased, although nonsignificant, in MCC950-treated LCNV tissues (3 animals/6 eyes per group). However, the volume of the CNV lesions were increased as shown in Fig. 3. (**C**) In addition, we did not observe significant changes in a-wave and b-wave amplitudes in ERG after MCC950 treatments, suggesting minimal effect on retinal cells (n = 6 eyes per group).

proangiogenic signaling molecule downstream of NLRP3 activation is IL-1β (29). In MCC950-treated mice, there was lower expression of both mRNA and secreted IL-1β protein (Fig. 5A, 5B), supporting that NLRP3 was inhibited by MCC950 despite an increase in total volume of the CNV lesions. Thus, our data suggest that this increased lesion size may not be directly related to IL-1β.

In conclusion, wet AMD is a disease that is characterized by choroidal neovascularization. The anti-VEGF treatment used to treat this condition is not effective for many AMD patients (30). Therefore. a greater understanding of choroidal neovascularization is needed to develop new potential therapies. Both NLRP3 and leukocytes have been investigated in the past for their roles in CNV. In our study, we show that NLRP3 regulates monocyte-derived macrophages and microglial recruitment in choroidal neovascularization. Therefore, understanding this relationship between NLRP3 and leukocyte recruitment could further lead to a clear understanding and eventually develop new therapies to protect against choroidal neovascularization.

DISCLOSURES

The authors have no financial conflicts of interest.

ACKNOWLEDGMENTS

We thank Dr. Carla J. Ramos for valuable assistance with the isolation of mRNA and protein samples from ocular tissues.

REFERENCES

1. Mitchell, P., G. Liew, B. Gopinath, and T. Y. Wong. 2018. Age-related macular degeneration. *Lancet* 392: 1147–1159.
2. Wong, W. L., X. Su, X. Li, C. M. G. Cheung, R. Klein, C.-Y. Cheng, and T. Y. Wong. 2014. Global prevalence of age-related macular degeneration and disease burden projection for 2020 and 2040: a systematic review and meta-analysis. *Lancet Glob. Health* 2: E106–E116.
3. Fleckenstein, M., T. D. L. Keenan, R. H. Guymer, U. Chakravarthy, S. Schmitz-Valckenberg, C. C. Klaver, W. T. Wong, and E. Y. Chew. 2021. Age-related macular degeneration. *Nat. Rev. Dis. Primers* 7: 31.
4. Tseng, W. A., T. Thein, K. Kinnunen, K. Lashkari, M. S. Gregory, P. A. D'Amore, and B. R. Ksander. 2013. NLRP3 inflammasome activation in retinal pigment epithelial cells by lysosomal destabilization: implications for age-related macular degeneration. *Invest. Ophthalmol. Vis. Sci.* 54: 110–120.
5. Paguaga, M. E., J. S. Penn, and M. I. Uddin. 2023. A novel optical imaging probe for targeted visualization of NLRP3 inflammasomes in a mouse model of age-related macular degeneration. *Front. Med. (Lausanne)* 9: 1047791.
6. Kelley, N., D. Jeltema, Y. Duan, and Y. He. 2019. The NLRP3 inflammasome: an overview of mechanisms of activation and regulation. *Int. J. Mol. Sci.* 20: 3328.
7. Malsy, J., A. C. Alvarado, J. O. Lamontagne, K. Strittmatter, and A. G. Marneros. 2020. Distinct effects of complement and of NLRP3- and non-NLRP3 inflammasomes for choroidal neovascularization. *Elife* 9: e60194.
8. Marneros, A. G. 2013. NLRP3 inflammasome blockade inhibits VEGF-A-induced age-related macular degeneration. *Cell Rep.* 4: 945–958.
9. O'Koren, E. G., R. Mathew, and D. R. Saban. 2016. Fate mapping reveals that microglia and recruited monocyte-derived macrophages are definitively distinguishable by phenotype in the retina. *Sci. Rep.* 6: 20636.
10. Kohno, H., H. Koso, K. Okano, T. R. Sundermeier, S. Saito, S. Watanabe, H. Tsuneoka, and T. Sakai. 2015. Expression pattern of Ccr2 and Cx3cr1 in inherited retinal degeneration. *J. Neuroinflamm.* 12: 188.
11. Pennesi, M. E., M. Neuringer, and R. J. Courtney. 2012. Animal models of age related macular degeneration. *Mol. Aspects Med.* 33: 487–509.
12. Shah, R. S., B. T. Soetikno, M. Lajko, and A. A. Fawzi. 2015. A mouse model for laser-induced choroidal neovascularization. *J. Vis. Exp.* 106: e53502.
13. Tobe, T., S. Ortega, J. D. Luna, H. Ozaki, N. Okamoto, N. L. Derevjanik, S. A. Vinores, C. Basilico, and P. A. Campochiaro. 1998. Targeted disruption of the FGF2 gene does not prevent choroidal neovascularization in a murine model. *Am. J. Pathol.* 153: 1641–1646.
14. Saederup, N., A. E. Cardona, K. Croft, M. Mizutani, A. C. Cotleur, C.-L. Tsou, R. M. Ransohoff, and I. F. Charo. 2010. Selective chemokine receptor usage by central nervous system myeloid cells in CCR2-red fluorescent protein knock-in mice. *PLoS One* 5: e13693.
15. Jiang, H., H. He, Y. Chen, W. Huang, J. Cheng, J. Ye, A. Wang, J. Tao, C. Wang, Q. Liu, et al. 2017. Identification of a selective and direct NLRP3 inhibitor to treat inflammatory disorders. *J. Exp. Med.* 214: 3219–3238.
16. Coll, R. C., A. A. B. Robertson, J. J. Chae, S. C. Higgins, R. Muñoz-Planillo, M. C. Inserra, I. Vetter, L. S. Dungan, B. G. Monks, A. Stutz, et al. 2015. A small-molecule inhibitor of the NLRP3 inflammasome for the treatment of inflammatory diseases. *Nat. Med.* 21: 248–255.
17. Ge, K., Y. Wang, P. Li, M. Li, W. Zhang, H. Dan, X. Hu, J. Zhou, Q. Yang, J. Wang, and Z. Song. 2022. Down-expression of the NLRP3 inflammasome delays the progression of diabetic retinopathy. *Microvasc. Res.* 139: 104265.

18. Sui, A., X. Chen, J. Shen, A. M. Demetriades, Y. Yao, Y. Yao, Y. Zhu, X. Shen, and B. Xie. 2020. Inhibiting the NLRP3 inflammasome with MCC950 ameliorates retinal neovascularization and leakage by reversing the IL-1beta/IL-18 activation pattern in an oxygen-induced ischemic retinopathy mouse model. *Cell Death Dis*. 11: 901.
19. Doyle, S. L., M. Campbell, E. Ozaki, R. G. Salomon, A. Mori, P. F. Kenna, G. J. Farrar, A.-S. Kiang, M. M. Humphries, E. C. Lavelle, et al. 2012. NLRP3 has a protective role in age-related macular degeneration through the induction of IL-18 by drusen components. *Nat. Med.* 18: 791–798.
20. Wooff, Y., S. M. Man, R. Aggio-Bruce, R. Natoli, and N. Fernando. 2019. IL-1 family members mediate cell death, inflammation and angiogenesis in retinal degenerative diseases. *Front. Immunol.* 10: 1618.
21. Cowan, P. J., D. Tsang, C. M. Pedic, L. R. Abbott, T. A. Shinkel, A. J. d'Apice, and M. J. Pearse. 1998. The human ICAM-2 promoter is endothelial cell-specific in vitro and in vivo and contains critical Sp1 and GATA binding sites. *J. Biol. Chem.* 273: 11737–11744.
22. Grossmann, R., N. Stence, J. Carr, L. Fuller, M. Waite, and M. E. Dailey. 2002. Juxtavascular microglia migrate along brain microvessels following activation during early postnatal development. *Glia* 37: 229–240.
23. Sorokin, S. P., and R. F. Hoyt. 1992. Macrophage development. 1. Rationale for using *Griffonia simplicifolia* isolectin B4 as a marker for the line. *Anat. Rec.* 232: 520–526.
24. Pawelec, P., M. Ziemka-Nalecz, J. Sypecka, and T. Zalewska. 2020. The impact of the CX3CL1/CX3CR1 axis in neurological disorders. *Cells* 9: 2277.
25. Espinosa-Heidmann, D. G., I. J. Suner, E. P. Hernandez, D. Monroy, K. G. Csaky, and S. W. Cousins. 2003. Macrophage depletion diminishes lesion size and severity in experimental choroidal neovascularization. *Invest. Ophthalmol. Vis. Sci.* 44: 3586–3592.
26. Sakurai, E., A. Anand, B. K. Ambati, N. van Rooijen, and J. Ambati. 2003. Macrophage depletion inhibits experimental choroidal neovascularization. *Invest. Ophthalmol. Vis. Sci.* 44: 3578–3585.
27. Xu, Y., K. Cu, J. Li, X. Tang, J. Lin, X. Lu, R. Huang, B. Yang, Y. Shi, D. Ye, J. Huang, S. Yu, and X. Liang. 2020. Melatonin attenuates choroidal neovascularization by regulating macrophage/microglia polarization via inhibition of RhoA/ROCK signaling pathway. *J. Pineal Res.* 69: e12660.
28. Gao, J. Y., J. Z. Cui, E. To, S. J. Cao, and J. A. Matsubara. 2018. Evidence for the activation of pyroptotic and apoptotic pathways in RPE cells associated with NLRP3 inflammasome in the rodent eye. *J. Neuroinflamm.* 15: 15.
29. Grebe, A., F. Hoss, and E. Latz. 2018. NLRP3 inflammasome and the IL-1 pathway in atherosclerosis. *Circ. Res.* 122: 1722–1740.
30. Mettu, P. S., M. J. Allingham, and S. W. Cousins. 2021. Incomplete response to anti-VEGF therapy in neovascular AMD: exploring disease mechanisms and therapeutic opportunities. *Prog. Retin. Eye Res.* 82: 100906.